Journal of Mammary Gland Biology and Neoplasia, Vol. 9, No. 4, October 2004 (© 2004)
DOI: 10.1007/s10911-004-1409-5

Viscoelastic Imaging of Breast Tumor Microenvironment With Ultrasound

Michael F. Insana,[1,3] Claire Pellot-Barakat,[1] Mallika Sridhar,[1] and Karen K. Lindfors[2]

Imaging systems are most effective for detection and classification when they exploit contrast mechanisms specific to particular disease processes. A common example is mammography, where the contrast depends on local changes in cell density and the presence of microcalcifications. Unfortunately the specificity for classifying malignant breast disease is relatively low for many current diagnostic techniques. This paper describes a new ultrasonic technique for imaging the viscoelastic properties of breast tissue. The mechanical properties of glandular breast tissue, like most biopolymers, react to mechanical stimuli in a manner specific to the microenvironment of the tissue. Elastic properties allow noninvasive imaging of desmoplasia while viscous properties describe metabolism-dependent features such as pH. These ultrasonic methods are providing new tools for studying disease mechanisms as well as improving diagnosis.

KEY WORDS: breast cancer; desmoplasia; molecular signaling; strain imaging; stromal reaction; pH imaging; tumor metabolism; ultrasound.

INTRODUCTION

Molecular signaling among epithelial, inflammatory and stromal tumor cells is a critical process guiding the growth and progression of breast carcinomas *(1)*. Epithelial-stromal signaling regulates tumor growth rate and helps determine the degree of invasiveness and metastatic potential. The type of tumor cells, their mixture, spatial organization, and biochemical activity each create the *tumor microenvironment* that prompts cell–cell and cell–matrix signaling. Current trends in cancer imaging aim to develop reliable and noninvasive methods for visualizing important structural and biochemical features of the tumor microenvironment in vivo and thereby provide unique tools for scientific investigation and improved diagnosis.

For nearly a century, breast cancer diagnosis has been based on information from clinical examinations combined with anatomical imaging, where tumor visibility depends on nonspecific contrast mechanisms, e.g., X-ray mammography. Mammography is often considered to be a more sensitive than specific indicator of cancer *(2)*. Recent discoveries in the molecular biology of breast cancer suggest that diagnostic specificity can be improved if we (a) directly image signaling molecules or associated receptors (*molecular imaging*) or (b) indirectly image the causes or effects of signaling and associated metabolic and structural responses (imaging features of the *tumor microenvironment*). We study mechanical properties of tissues affected by pO_2, pH,

[1] Department of Biomedical Engineering, University of California, Davis, California.
[2] Department of Radiology, University of California–Davis Medical Center, Sacramento, California.
[3] To whom correspondence should be addressed at Department of Biomedical Engineering, University of California, Davis, California 95616; e-mail: mfinsana@ucdavis.edu.

Abbreviations used: DCIS, ductal carcinoma in situ; ECM, extracellular matrix; IDC, infiltrating ductal carcinoma; ILC, infiltrating lobular carcinoma; MMP, matrix metalloproteinase; MRI, magnetic resonance imaging; PET, positron emission tomography; pHe, extracellular pH; SNR, signal-to-noise ratio; US, ultrasound; VEGF, vascular endothelial growth factor.

metabolic rate, and mechanical stress since these features are environmental stimuli promoting or inhibiting signaling processes that influence tumorigenic phenotypes *(3,4)*.

One type of molecular imaging of cancer is based on the angiogenic signaling that involves $\alpha v\beta 3$-integrins. It uses integrin-based probes and a variety of imaging modalities *(5,6)*. Other types target gene expression and protein function *(7,8)*. The heart of molecular imaging is the contrast enhancement obtained from sophisticated imaging probes, which are circulating molecular complexes that adhere to specific sites in the body and emit or reflect observable energy. Any modality can be used for molecular imaging without spatially resolving molecular-scale events provided there is specific probe affinity for the target (large object contrast) and sufficiently high SNR (low image noise).

Probe-based imaging of the tumor microenvironment can also improve the specificity of the diagnostic information. Metabolic imaging is an example where 2[^{18}F]-fluoro-deoxy-D-glucose probes sensed by PET scanners generate high object contrast by exploiting the large differential uptake of the glucose probe into cancer cells. PET imaging has been found to provide quantitative information that correlates well with histological features describing the progression of ductal carcinoma in situ (DCIS) to infiltrating ductal carcinoma (IDC) in breast cancer mouse models *(9)*.

Our approach is to use ultrasound (US) to image mechanical properties of tumors that are determined by the microenvironment. US provides information with little or no risk to the subjects, at relatively low cost compared with other modalities, and with high temporal resolution to observe dynamic processes. Viscoelastic imaging of breast tumors aims to observe the *effects* of molecular signaling and cell metabolism by exploiting the large natural contrast in mechanical material properties that exists between cancerous and noncancerous soft tissues *(10,11)*.

TUMOR ELASTICITY AND THE MICROENVIRONMENT

Breast adenocarcinomas begin as a group of genetically altered epithelial cells mixed with stromal cells *(1)*. It is thought that tumor formation depends on the ability of epithelial cells to transform local stromal cells. For example, fibroblasts and other progenitor cells are converted into myofibroblasts, which comprise as much as 90% of the tumor mass *(12,13)*. The effect of epithelial cell signaling on stromal cells is referred to as the *stromal response*. Myofibroblasts have high rates of proliferation and protein expression, including growth factors. From initiation through late stage development, IDC tumor-associated myofibroblasts secrete enormous amounts of collagen and extracellular matrix (ECM) proteins that condense and contract due to a smooth-muscle actin-myosin component. One consequence of the stromal reaction is *desmoplasia*, which is responsible for the scirrhous properties of palpable tumors. In the highly vascularized desmoplasia of advanced IDC, myofibroblast activity shifts outward to the growing edge *(1)*, producing a twofold *(14)* to more than 10-fold *(11)* increase in the stiffness of tissues surrounding the tumor.

The natural object contrast for elasticity imaging is thus greater than that for mammography or sonography, but the nature of the contrast mechanisms is poorly understood and the subject of much current research.

ULTRASONIC ELASTICITY IMAGING

During manual palpation, a physician's finger tips press into the skin surface to deform the tissues being examined and sense variations in elasticity. The deformation generates a mechanical stress field in the tissue beneath the fingers that varies according to the elastic modulus of the medium below and the shape of the internal structures, referred to as boundary conditions. Stress (σ = force per unit area) arises from the elastic property of soft tissues that resists deformation in proportion to the amount applied. The same finger tips then sense tissue "stiffness" from the intensity of the restoring force propagated to the fingers from the medium immediately below. The restoring force increases with the proximity of the stiff lesion to the skin surface. Despite low sensitivity for deep objects and little spatial resolution, manual palpation has been part of the physical exam for two millennia primarily because of the large stiffness contrast found in many cancerous lesions and other inflammatory processes.

Elasticity imaging *(14–25)* employs similar principles but with greater sensitivity for deep structures and with spatial resolution comparable to the host modality. It is often referred to as palpation by remote sensing, where tactile sensing is replaced by a medical imaging device. The basic procedure is

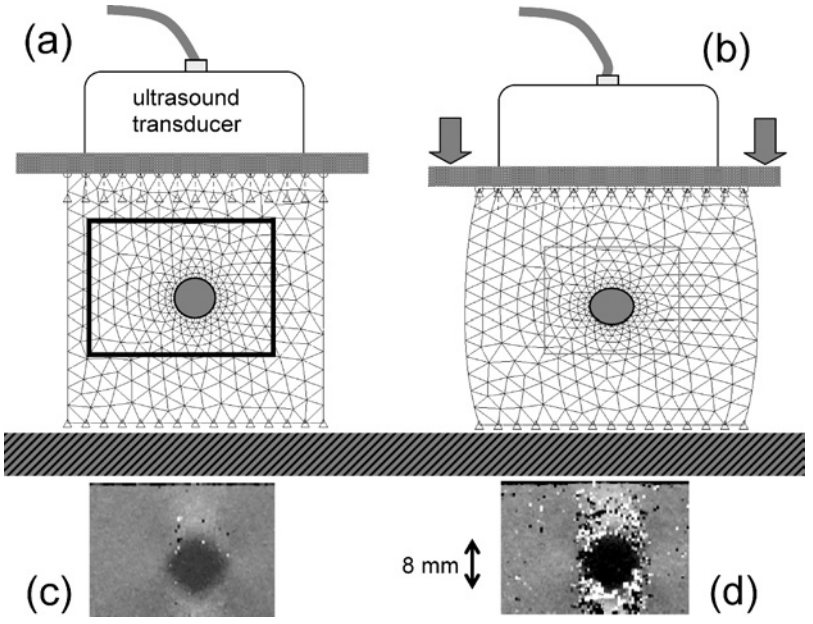

Fig. 1. A static elasticity imaging technique is illustrated using a tissue-mimicking phantom with an 8-mm-diameter stiff inclusion and a clinical ultrasound scanner. (a) Image data are acquired from a subregion (boxed area) before deformation. (b) An external force is applied by the imaging transducer and a second scan is obtained immediately. A speckle tracking algorithm compares echo signals about the mesh points to compute displacements. Strain images are found from the derivative of interpolated displacements in the direction of the beam (vertical axis). (c) Applying a small compressive force yields low image contrast but little decorrelation noise. (d) Applying three times the force triples the image contrast for the inclusion but generates decorrelation noise unless more sophisticated and time-consuming techniques are applied.

simple: a medical image is recorded, a mechanical force deforms the imaged region by a small amount, and the tissue is imaged again (Fig. 1). Region-by-region comparisons of radio-frequency echo signals in the pre- and postdeformation image frames reveal the displacement field *(18)*, from which strain (ε = spatial variation in displacement) is computed. If the applied stress field in the medium can also be estimated, then a mechanical modulus (geometry-independent stiffness property of tissue) can be estimated from the strain. Large deformations produce large image contrast and, unfortunately, significant decorrelation noise as seen by comparing Fig. 1(c) and (d), unless more sophisticated techniques are applied (not shown). Much of our previous research on elasticity imaging has been to learn how to deform heterogeneous tissues and then detect that deformation in a manner that maximizes lesion visibility *(18)*. Generally, system features that improve ultrasonic resolution also improve strain resolution and motion sensitivity, but also increase noise and decrease depth of penetration. These factors combine to determine lesion visibility.

Depending on the nature of the applied stress, boundary conditions, and allowable image reconstruction time, various mechanical moduli and strains are computed and mapped into images to reveal the material properties of the examined region of the body *(24)*. Strain images can be formed at real-time rates *(25)* and therefore they are the most common form of elasticity imaging. As shown in Fig. 1, stiff tumors are often displayed as dark regions (low strain) in a bright background.

Static elasticity imaging techniques yield those elastic properties of tissues that are made visible when a steady mechanical force is applied and held *(16,26,27)*. When it is suddenly applied to the tissue, strain is estimated immediately before viscous responses can engage or after a long delay to allow the viscous flows to settle. Either way, the time-varying constitutive equation relating stress σ and strain ε under these quasi-static conditions may be

given as $\sigma(t) = G_e(t)\varepsilon(t)$, where G_e is called the elastic shear modulus. Other investigators apply a stress field that varies sinusoidally over time while tracking movements sonically *(28)*, ultrasonically *(29)* or with MR methods *(30–32)*. Steady-state dynamic conditions are assumed to adopt the frequency domain constitutive equation $\sigma(\omega) = G^*(\omega)\varepsilon(\omega)$, where G^* is the complex shear modulus that depends on the frequency of the stimulus ω. Static and dynamic techniques provide different features of the material properties of tissue, and it is still unknown how each feature describes the tumor microenvironment.

Each imaging approach has a demonstrated ability to aid in the detection and classification of lesions. Garra et al. *(33)* studied 50 patients and found that the desmoplastic reaction surrounding many common malignant breast tumors was a distinctive feature of strain images useful for differential diagnosis. Because strain and B-mode pixels are spatially registered, they were able to show that malignant lesions appear larger in strain than they do in B-mode while benign lesions are the same size. The larger size corresponds to desmoplasia surrounding malignant lesions that cannot be seen using any other imaging method. Garra's original finding of increased diagnostic specificity was supported by a recent independent study *(34)*. Others found ultrasonic strain imaging useful for detection but were unable to assess its ability to differentiate malignant and benign lesions *(35)*. Still others working with MRE methods found malignant lesions to be twice as stiff as benign lesions *(36)* and malignancies more than four times stiffer than the surrounding parenchymal tissue *(31)*, in agreement with mechanical tests on tissue samples *(11)*. Clearly the enormous elastographic contrast for cancer can be exploited using either US or MR images but a consistent picture of the underlying mechanisms has yet to emerge. Both modalities are able to detect submicron movements. MR allows data acquisition from a finely sampled tissue volume, which is ideal for imaging complex 3D deformations, while US currently is limited to imaging deformation in a plane. However US often provides higher temporal resolution for acquisition and therefore allows tracking of fast, nonrepetitive physiological deformations.

Recently, US techniques using acoustic radiation force to apply a local impulse stress stimuli *(37)* were developed. Also harmonic shear-wave stimuli coupled with very fast ultrasonic acquisition (6000 frames/s) *(38)* to image the moving shear waves can be used to visualize viscoelastic (time varying) properties independent of boundary effects. While both of these methods have significant potential for providing unique biophysical information about disease, they require major modifications to current instrumentation or risky high intensity sound pulses to implement. Most likely, it will be a combination of several mechanical properties that will reveal relationships between disease processes and tissue viscoelastic properties.

ULTRASONIC SCATTERING AND TISSUE ELASTICITY

To understand why ultrasound is well suited to imaging deformation, we review some of the tissue properties that interact with the sound field and how the associated elastic properties are related. Ultrasonic echo signals can be used to track tissue motion because the mechanical properties that determine wave propagation through the body are not the same as those that determine stiffness; that is, echogenicity is unaffected by most tissue deformations we can apply. Echo signals vary with the material properties that determine sound speed. The "speed of ultrasound" usually refers to the speed of compressional waves c; it is a function of mass density ρ and adiabatic bulk compressibility K via $c^2 = K/\rho$. Since ρ and K vary little throughout the various tissues of the breast, c is constant within 6% of the mean. Furthermore, it is known that c and the ultrasonic absorption α do not significantly depend on anatomic structures at or above the cellular level; short-range molecular interactions regulate sound speed and absorption *(39)*. Since absorption accounts for about 97% of sound-tissue interactions, most of the energy transmitted is deposited as heat and cannot be imaged. About 3% of the transmitted energy is scattered, and only a fraction of the scattered energy is detected by the transducer to form an echo signal for imaging. Unlike absorption, ultrasonic scattering occurs at *surfaces* of anatomic structures. At diagnostic frequencies, most scattering occurs at boundaries between microscopic volumes with different acoustic impedances as defined by $z = \rho c = K/c$. Consequently, only those tissues containing numerous tiny surfaces of varying acoustic impedance appear in sonograms. Collagenous stromal cells and lipid surfaces are sites of the greatest tissue scattering *(40)*. Edematous lesions having lower scatterer density provide the negative object contrast seen often for breast lesions in sonography. Tracking the spatial

redistribution of tissue scatterers following deformation is the task of the strain imaging algorithm.

Of the four types of body tissues—mesenchymal, epithelial, reticuloendothelial, and nervous—ultrasound is most sensitive to the mesenchyma (connective tissue stroma, microcalcifications, muscle, lymphatics, and fibroblasts). Sound scattered at surfaces of these breast microstructures gives rise to echo signals that are very sensitive to the size, orientation, and number density of these components *(41)*. Most breast cancers begin in the epithelial cells, and the US is most sensitive to tissue stroma. Consequently it is the relationship between cancerous epithelial cells and the stromal response that gives ultrasound its diagnostic capabilities. Ultrasonic imaging can accurately track local tissue motion on the order of microns in real-time, with spatial resolution on the order of hundreds of microns, and without affecting stiffness. Conventional sonography and other imaging modalities cannot directly visualize tissue stiffness of viscoelastic properties. Elasticity imaging requires there to be measurable motion of scatterers between frames of a temporal sequence of images.

K and ρ discussed above govern ultrasonic wave propagation because of the short time scale over which mechanical forces act: at 10 MHz, particle forces reverse polarity every 100 ns. K describes the relative *change in volume* that occurs when stresses are applied to a medium. Slowly varying stress stimuli that deform tissues, as in the strain imaging experiment illustrated in Fig. 1, allow the medium time to respond. These responses are governed by the shear modulus G that describes the *change in shape* of tissues subjected to stress. The high water content makes tissues nearly incompressible (they change shape but not volume when stressed). Consequently, the shear and elastic moduli are proportional in most biological tissues, $E = 3G$. Shear deformation waves travel at the much slower shear wave speed $c_s^2 = G/\rho$ *(42)*, where $c_s/c \cong 0.02$ *(43)*.

How accurately can the intrinsic mechanical properties of breast tissues be estimated considering the enormous heterogeneity and unknown microstructure? From a precise materials science perspective, such measurements are difficult or impossible to make accurately. To understand this point, one must review the theory of viscoelastic solids *(44)*, which shows that the accuracy of material property measurements depends on sample geometry, spatial distribution of the applied mechanical stimulus, and boundary conditions. We are attempting to estimate average properties of complex composite biomaterials whose stiffness depends on the shape and orientation of unknown internal structures, not all of which can be sensed with US. The conditions required for measuring elastic moduli that define "stiffness" usually cannot be obtained or controlled experimentally, and so accurate measurements of rigorously defined mechanical moduli are rarely possible. How then should we design experiments and instruments to study complex biological tissues?

The solution is to maximize the sensitivity and specificity for visual classification rather than attempt to accurately measure intrinsic material properties. The task determines the specifications for strain imaging systems and associated algorithms *(45)* and defines criteria for image quality assessments and performance *(46)*. One important task is detection of 2–10 mm breast lesions where the shear modulus is estimated to vary 100% from the background *(11)*. Breast strain imaging of small lesions is often noise limited, and therefore the best imaging techniques strive to achieve a large strain SNR at acceptable values of contrast and spatial resolution. We are currently testing the sensitivity of strain ε to measure features of the tumor microenvironment; e.g., let θ_1 = extracellular pH and θ_2 = collagen density, where $\theta = (\theta_1, \theta_2)$ is a feature vector. System parameters are set to maximize sensitivity to these features, viz., to maximize $\partial\varepsilon/\partial\theta_i$, for in vivo imaging conditions.

CLINICAL IMAGING: EARLY RESULTS

The literature contains preliminary clinical studies evaluating the use of ultrasonic elasticity imaging to discriminate palpable breast lesions *(33,47)*. As stated earlier, these investigators find large negative contrast for both benign and malignant lesions, and that benign lesions appear the same size in strain images as they do in sonograms and mammograms. Malignant lesions, however, appear significantly larger in strain images, presumably because strain is uniquely sensitive to the desmoplasia that surrounds the lesion.

We selected a different patient population for our preliminary clinical study. These patients had *nonpalpable* suspicious masses that were discovered on screening mammograms. Example of three nonpalpable lesions, one benign and two malignant, are shown in Fig. 2 for three imaging techniques.

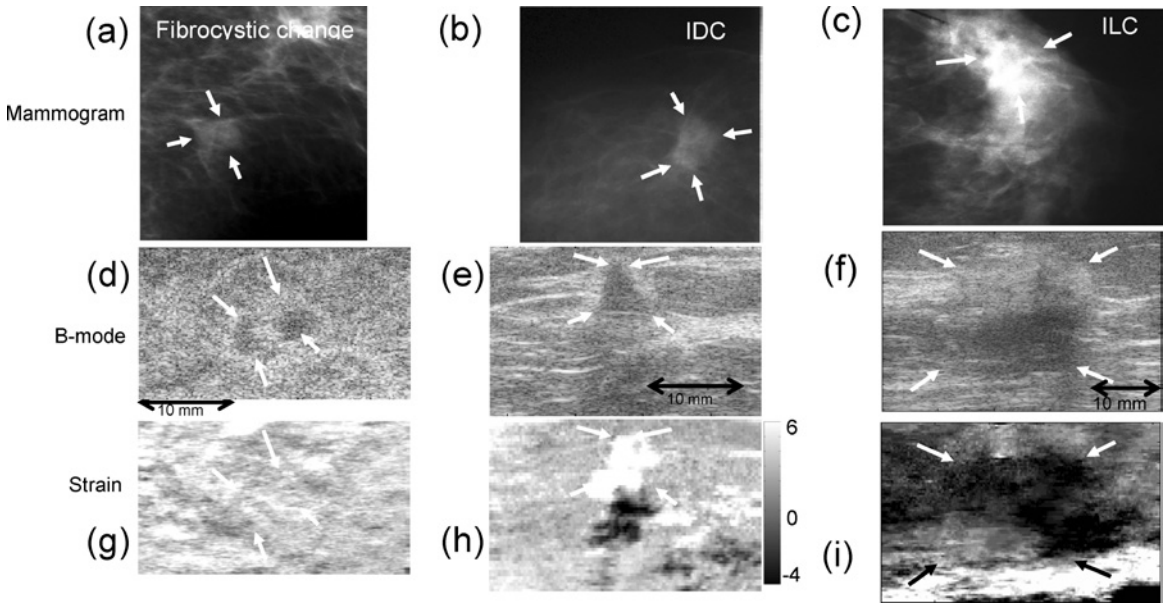

Fig. 2. Mammograms (a,b,c), sonograms (d,e,f), and elastograms (strain images) (g,h,i) of breast lesions recorded from three female patients, in vivo. These lesions were nonpalpable and first detected by mammography. The diagnosis for each lesion was determined by ultrasound guided core biopsy. Although the echogenicities are similar, the benign lesion (fibrocystic change with apocrine metaplasia; 47 years) does not appear in the corresponding strain image (g); the IDC lesion (SBR grade II 95% and DCIS 5% without microcalcifications; 48 yrs) appears much softer than its background (h), and the ILC lesion (SBR Grade I with Lobular Carcinoma in situ; 66 years) is larger, somewhat stiffer than its background, and heterogeneous (i). Soft lesions (bright regions in strain images) generate artifacts appearing as dark copies immediately below. The gray scale bar indicates percent strain, where positive values are compressive and negative values are tensile. The dimensions apply to sonogram/elastogram pairs; both are spatially registered. Mammograms are acquired from different orientations and do not correspond in scale to the sonograms and elastograms.

X-ray mammograms (Fig. 2(a)–(c)), sonograms (Fig. 2(d)–(f)) and strain images (Fig. 2(g)–(i)) are compared; the latter two are spatially registered. The mammograms display hyperdense soft tissue masses, while the sonograms show hypoechoic lesions. The differences in elastographic appearances in these examples are much greater. The fibrocystic lesion generates little detectable strain contrast, indicating that it has the same stiffness as the background, as expected for many benign masses (Fig. 2(g)). Conversely, the nonpalpable IDC lesion (Fig. 2(h)) appears much softer (brighter) than its background. The dark regions mirrored below bright regions are artifacts common to soft lesions in strain images. It is reportedly rare to see soft malignant lesions. We conjecture that it may appear soft if it is in a fast growing, angiogenic phase, where MMPs have eroded the ECM as vessels develop; other factors related to the tumor histology or the surrounding tissue environment may be influential as well. Further study in animal models is required to explain this source of contrast. The ILC lesion appears much stiffer (darker) than its background on the elasticity image (Fig. 2(i)). It also appears larger than on the sonogram (Fig. 2(f)), which seems to indicate the presence of desmoplasia. These examples demonstrate that deep or small nonpalpable lesions may clearly show contrast in strain images. Figure 2 shows that changes in collagen density and edema that generate sonographic contrast can be nonspecific for discrimination. However the long-range connections among collagen fibers that determine tissue elasticity may provide much greater contrast. There are not enough data to know if elasticity imaging is more specific than other methods for some patient groups, such as women with nonpalpable breast masses, but the results thus far are promising.

GELATIN AS A TOOL FOR EXPLORING TISSUE VISCOELASTICITY

Most of our past efforts have been to understand the physics of tissue mechanics and develop instrumentation and algorithms to exploit this information.

Water-based gelatin has become the test medium of choice in imaging development because of its similarities to many parenchymal tissues, including breast. Material properties of tissues, such as water structuring, partitioning of solutes, resistance to freezing and viscoelasticity, have traditionally been studied using water-based gelatin as an experimental model *(48)*. Gelatin has also been a staple in the development of basic ultrasonic imaging *(49,50)*, but the extent of the similarity to tissues has yet to be fully explored in the context of elasticity imaging.

Ultrasonic phantom technology is based on a century-old literature on gelatin science *(51,52)*. Animal hide gelatin is obtained from skin and other connective tissues by partial hydrolysis of collagen. Powdered gelatin available commercially is derived from long macromolecules that are highly cross-linked with covalent bonds that form slowly over the lifetime of the animal, and also through weaker secondary forces. The manufacturing process extracts collagen by heating and chemical hydrolysis that breaks down these covalent bonds and shortens the fibers.

Tissue-like phantoms are constructed by mixing powdered gelatin with an alcohol-water solution (alcohol is added to adjust sound speed) and heating to a temperature between 35°C and 40°C to free and eliminate dissolved gasses. Fine inert particles are added to provide ultrasonic absorption and scattering, and the mixture is cooled to initiate gelation. Cooling molecules reform the original triple-helical fiber structure and then aggregate to form small locally ordered regions (crystallites). Aggregates polymerize through secondary forces to form a weak random network of collagen fibers with charged hydrophilic surfaces. The collagen fibers interact very little with sound waves but are responsible for viscoelastic properties. In contrast, the suspended particles contribute most of the scattering and almost nothing to the shear modulus *(49)*. The network structure is in constant flux at room temperature, thus pure gelatins melt at body temperature. Stability is obtained by chemically cross-linking the aggregates using aldehydes, thus adding strong covalent bonded links to weaker hydrogen bonded links.

The weak long-range connections in gelatin create a random 3-D mesh that traps water and scattering particles (Fig. 3(a)). Under constant uniform stress (Fig. 3(b)), the cross-links initially stretch, giving an instantaneous elastic response. Trapped water begins to flow, generating a viscous response that stabilizes on the scale of milliseconds to seconds. The flow rate depends on the surface charge density and proximity of the collagen fibers, which is affected by pH and polymer fiber density. Polar water molecules closest to straight fiber segments (see inset to Fig. 3(a)) align to form the more viscous *structural or vicinal water (53)*. Consequently, dense collagenous structures behave as stiff polymers or hydrogels in which water viscosity determines the flow rate under stress. Finally, the stretched hydrogen-bonded cross-links release and are reformed at a lower (relaxed) energy state (Fig. 3(c)) generating a second, slower viscous response that stabilizes on the scale of 10–100 s. Cross-link relaxation rates also depend on polymer surface change density. We can control the three structural components of gelatin (covalent bonding of collagen, secondary bonding of cross-links, and structured water) that determine the viscoelastic properties by varying pH (charge density), thermal history (collagen fiber length and linearity), adding chemical cross-linking agents and applying mechanical stresses *(54)*.

We conjecture that gelatin may be used as a straightforward physical model for understanding time-dependent strain measurements—the viscoelastic response—of soft biopolymer solids, including breast tissues. With it, controlled experiments can be conducted to test ideas that explain the image data often observed.

Figure 4(a) is an example of ultrasonic image data obtained from a gelatin phantom where the stiff central target has three times the gelatin concentration of the background. Higher collagen density is a simple model for fibrosis and desmoplasia in breast disease. During a strain imaging experiment, we first record echo data at $t < t_0$, apply and hold a compressive stress beginning at time $t = t_0$, and then record another echo frame at $t > t_0$. The pair of echo frames is processed to compute the strain image. Figure 4b is a plot of the applied stress (of amplitude σ_0, dashed line), the average measured strain ε inside the stiff target (dotted line), and average measured strain in the surrounding background (solid line). The shape of the curves is explained by the theory of viscoelastic solids (44), which provides a constitutive equation that describes changes in gel strain observed over time and space,

$$\varepsilon(t, x) = \varepsilon_0(x) + \varepsilon_1(x)\upsilon_1(t, t_0, T_1) + \varepsilon_2(x)\upsilon_2(t, t_0, T_2).$$

The three terms comprises elastic factors $\varepsilon_i(x) = E_i(x)\sigma_0(x)$ that are independent of time and

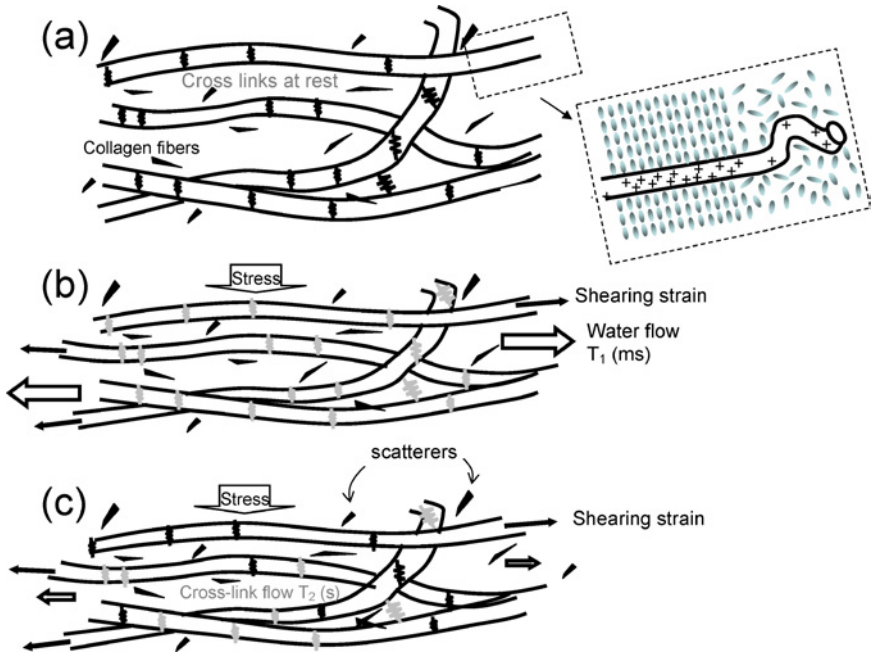

Fig. 3. Changes to a collagen network of gelatin subjected to a step stress are illustrated. The network is shown before deformation in (a), immediately after deformation in (b), and after viscous mechanisms have decayed in (c). Gray springs denote strained cross-links under stress (high energy state) and black springs represent those H-bonded cross-links at rest after decay (low energy state). The black spots are scattering particles; typically graphite. The inset on (a) illustrates structured water near linear segments of collagen fibers.

viscous factors $\upsilon_i(t) = (1 - \exp(-(t - t_0)/T_i)$ that are independent of location. The observed strain and corresponding lesion contrast depend on the time

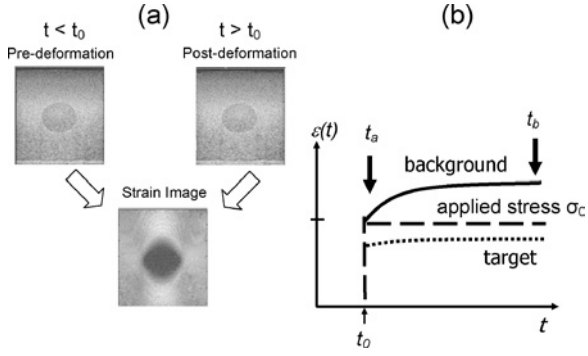

Fig. 4. (a) Strain image formation from two echo frames recorded from a tissue-like gelatin phantom is shown. Sonographic contrast from the 15-mm-diameter inclusions arises from differences in scattering particle concentrations, whereas strain contrast depends on collagen fiber cross-linking. (b) The average strains from small regions inside and outside the target are plotted as a function of time to illustrate the one elastic and two viscoelastic components of the mechanical response to the step stress stimulus.

that the postdeformation frame is acquired. For example, acquiring the postdeformation echo frame at $t = t_a \ll T_1, T_2$, we find $\varepsilon(t_a, x) \cong \varepsilon_0(x)$, since $\upsilon_1 = \upsilon_2 \cong 0$. However, delaying the acquisition to $t = t_b \gg T_1, T_2$ allows the deformed medium time to engage the two viscous responses specified by the relaxation times T_1 and T_2. The associated constitutive equation is $\varepsilon(t_b, x) \cong \varepsilon_0(x) + \varepsilon_1(x) + \varepsilon_2(x)$ since $\upsilon_1 = \upsilon_2 \cong 1$. From a time series of strain images acquired between t_a and t_b, the relaxation time constants T_1 and T_2 can be estimated. The situation is analogous to magnetic resonance imaging (MRI), where the net magnetization is determined by proton density that varies with time depending on spatially varying magnetic relaxation parameters. Because of what we learned from hydrogels and their assumed similarity to tissue stroma, we propose the use of ε_0, T_1, and T_2 to form three parametric images describing viscoelastic properties of tissues *(55)*. Unique information will be obtained if mesenchymal viscoelasticity is found to be a sensitive indicator of the tumor microenvironment, particularly for desmoplasia, fibrosis, and metabolic/perfusion changes that regulate extracellular pH.

From the plot, it is easy to see that target contrast varies as a function of time. The contrast we see in the strain image of Fig. 4(a) depends not only on the elasticity of the object but on the viscous creep from the water flow and cross-link relaxation.

CLINICAL IMPLICATIONS OF THE TUMOR MICROENVIRONMENT

Increasingly, investigators have focused on the microenvironment of tumors to understand the variable rates of metastatic progression and therapeutic responses *(56,57)*. The microenvironment is often characterized by the spatial distribution of the partial pressure of oxygen (pO_2) and extracellular pH (pHe), since it is known that hypoxia and acidity have significant influence on cell death and growth rates *(57,58)*. Hypoxia results primarily from poor perfusion and acidosis from elevated cell metabolism, although these effects are dependent.

Hypoxia and acidity lead to more aggressive cancer cell phenotypes. Both contribute directly to increased progression of cells from benign hyperplasia to metastatic neoplasia *(59)* and indirectly by natural selection. Low pO_2 and low pHe conditions have been shown to reduce DNA repair in tumors, which are already genomically highly unstable *(60)*. Thus there is an increase in mutation rate and cancer cell proliferation. Mechanisms that lead to more aggressive tumor behavior are complex and poorly understood.

Hypoxia and acidosis also increase the resistance of tumors to therapies. The poorly-formed chaotic patterns of tumor vasculature are responsible for regions of low pO_2 within solid tumors. Low oxygen pressures yield low numbers of reactive species during radiation therapy that are needed to damage macromolecules and membranes of tumor cells effectively. Consequently, hypoxic tumor cells are 3–5 times more resistant to ionizing radiation compared to well-oxygenated cells *(61)*. Low pHe also inhibits radiotherapy *(62)* while mysteriously enhancing hyperthermia *(63)*. It can be critically important to monitor changes in tumor microenvironment in individual patients over time to assess and then evaluate treatments for potentially aggressive malignancies.

VISCOELASTIC MEASUREMENTS IN TISSUE-LIKE GELATIN

We have not imaged relaxation time constants for enough patients to report results at this time. However feasibility studies in gelatin are very encouraging. Figure 5 displays images of elastic strain ε_0 and the two viscous time constants: T_1 indicates fast creep due to water flow and T_2 indicates slow creep due to the relaxation of stretched polymer cross-links. As in Fig. 4, the 15-mm-diameter phantom target has three times the gelatin concentration of the background to mimic the object contrast for stiff IDC breast samples relative to normal glandular tissues *(11)*. Details of the phantom and measurements in Fig. 5 are given in reference *(55)*. We compressed the phantom 10% and applied multicompression and temporal averaging techniques *(64)* to enhance strain contrast without generating decorrelation noise. In the ε_0 images of Fig. 5(a), the darker regions indicate low strain and thus stiffer regions similar to

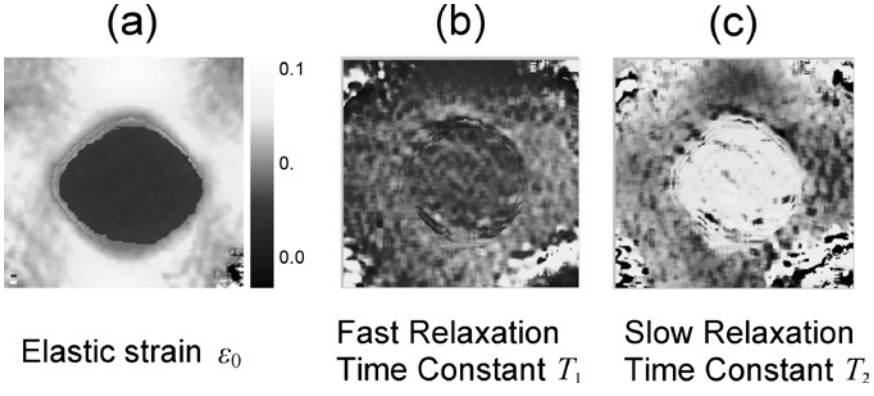

Fig. 5. Viscoelastic images of the phantom shown in Fig. 4. The range for ε_0 image is shown. The range for the T_1 image is 100 ms to 5 s, and the range for the T_2 image is 20—200 s.

the gray-scale strain image in Fig. 4. Higher gelatin concentration in the target increases gel stiffness as expected. Stiff target regions generate greater-than-average strains in regions immediately above and below the target when subjected to a uniform stress from above or below.

The T_1 image suggests that water flow during compression is about the same throughout the phantom. This surprised us, since closer proximity of fibers in the target was expected to increase the viscosity of vicinal water. Apparently the applied stress was not sufficient to fully engage the relaxation mechanism and generate contrast from spatial variation in water flow. However, the same target in the T_2 image appears significantly brighter than the surrounding background, suggesting that the hydrogen-bonded cross-links relax more slowly in higher concentration gels. Such a response is consistent with the fact that closer collagen fiber proximity increases cross-link density. It seems that gelatin is a tractable model for developing imaging methods.

The gelatin phantom data of Fig. 5 shows that viscoelastic imaging is sensitive to changes in polymer density. Other studies *(55,65)* have shown equally high sensitivity to pH changes in both gelatin and tissue. For example, we observed significant T_1 image contrast in regions of liver tissue where acids were injected *(65)*. These data suggest it is possible to image spatial variations in water flow rates with ultrasound. Rheometer measurements provide an independent source of data on gel properties under near-ideal geometric measurement conditions—effectively a gold standard measurement by which imaging methods can be evaluated *(55)*.

Our current research effort includes investigations to determine whether microenvironmental changes affect the polymer structure of breast tumor stromal collagen in a manner that viscoelasticity imaging can detect. It is known that natural polymers, like the proteins in stromal tissue, also have charged hydrophilic surfaces. Charges arise at side chains on the amino acid backbone. These generate hydrogen-bond cross-links between polymer fibers that resist deformation for a time and decay. Also these charged surfaces adsorb water molecules because of their polar charge. The hydrophilic nature of charged surfaces aligns water molecules to form layers. Recent experiments suggest that structured water is 10–100 times more viscous than bulk water *(53)*. Hence tumor tissues are technically gels, and gels are viscoelastic solids. Their elastic properties are determined principally by covalent bonds between polymer chains that are unchanged during mild deformations. Viscous properties, however, are determined by structured water and cross-linked side chains that are altered when stressed. Similarities between the physical chemistry of congealed gelatin and breast stroma are many.

SUMMARY

The methods described in this paper outline new applications of ultrasonics to the imaging of breast tissue viscoelastic properties. Advances in the molecular biology of cancer suggest that the tumor microenvironment can be a regulator of the signaling pathways that control tumor growth, metastatic risk, and responses to traditional therapeutics. The water-based gelatin media now used to evaluate imaging techniques is also guiding our investigations aimed at understanding the mechanisms responsible for tissue viscoelasticity. This truly interdisciplinary research has much promise as a noninvasive tool for studying the basic science of breast cancer in vivo.

The ultimate clinical role for breast viscoelasticity imaging is early detection of developing tumors that have a stromal reaction or are altering their environment but have not yet had mutated epithelial cells breach the ductal basement membrane. Once breached, epithelial cells mix with highly active stromal cells that accelerate tumor progression and metastasis. Successful detection at that this early stage of tumor development could improve outcome.

ACKNOWLEDGMENTS

The authors gratefully acknowledge contributions from Drs Scott Simon at UCD and Patrick Von Behren at Siemens. This work was supported in part by grants from the National Institutes of Health R01 CA82497 and Siemens Medical Solutions, Ultrasound Group.

REFERENCES

(1) Elenbaas B, Weinberg RA. Heterotypic signaling between epithelial tumor cells and fibroblasts in carcinoma formation. Exp Cell Res 2001;264:169–84.

(2) Buchbinder SS, Leichter IS, Lederman RB, Novak B, Bamberger PN, Sklair-Levy M, Yarmish G, Fields SI. Computer-aided classification of BI-RADS category 34 breast lesions. Radiology 2004;230(3):820–3.

(3) Carmeliet P, Jain RK. Angiogenesis in cancer and other diseases. Nature 2000;407:249–57.

(4) Kim JB, Stein R, O'Hare MJ. Three-dimensional in vitro tissue culture models of breast cancer—A review. Breast Cancer Res Treat 2004;85:281–91.
(5) Dayton P, Pearson D, Clark J, Simon S, Schumann P, Zutshi R, Matsunaga T, Ferrara K. Ultrasonic detection of alpha Vbeta3 expressing-cells with targeted contrast agents. Molec Imag 2004;3(2):125–34.
(6) Sipkins DA, Cheresh DA, Kazemi MR, Nevin LM, Bednarski MD, Li KC. Detection of tumor angiogenesis in vivo by alphaVbeta3-targeted magnetic resonance imaging. Nat Med 1998;4:623–6.
(7) Winnard P Jr, Raman V. Real time non-invasive imaging of receptor-ligand interactions in vivo. J Cell Biochem 2003;90(3):454–63.
(8) Sullivan DC. Challenges and opportunities for in vivo imaging in oncology. Technol Cancer Res Treat 2002;1(6):419–22.
(9) Abbey CK, Borowsky AD, McGoldrick ET, Gregg JP, Maglione JE, Cardiff RD, Cherry SR. In vivo PET imaging of progression and transformation in a mouse model of mammary neoplasia. Proc Natl Acad Sci USA 2004;101:11438–43.
(10) Sarvazyan AP, Skovoroda AR, Emelianov SY, *et al.* Biophysical bases of elasticity imaging. In: Jones JP editor. Acoustical Imaging. Vol 21. New York: Plenum Press; 1995; p. 223–40.
(11) Krouskop TA, Wheeler TM, Kallel F, Garra BS, Hall TJ. Elastic moduli of breast and prostate tissues under compression. Ultrason Imag 1998;20:260–74.
(12) Dvorak HF. Tumors: Wounds that do not heal. Similarities between tumor stromal generation and wound healing. N Engl J Med 1986;315:1650–9.
(13) Schürch W, Seemayer TA, Gabbiani G. The myofibroblast: A quarter century after its discovery. Am J Surg Pathol 1998;22:141–7.
(14) Lorenzen J, Sinkus R, Lorenzen M, Dargatz M, Leussler C, Roschmann P, Adam G. MR elastography of the breast: preliminary clinical results. Rofo Fortschr Geb Rontgenstr Neuen Bildgeb Verfahr 2002;174:830–4.
(15) Tristam M, Barbosa DC, Cosgrove DO, Nassiri DK, Bamber JC, Hill CR. Ultrasonic study of in vivo kinetic characteristics of human tissue. Ultrasound Med Biol 1986;12:927–37.
(16) O'Donnell M, Skovoroda AR, Shapo BM, Emelianov SY. Internal displacement and strain imaging using ultrasonic speckle tracking. IEEE Trans Ultrason Ferroelec Freq Control 1994;41:314–25.
(17) Muthupillai R, Lomas DJ, Rossman PJ, Greenleaf JF, Manduca A, Ehman RL. Magnetic resonance elastography by direct visualization of propagating acoustic strain waves. Science 1995;269:1854–7.
(18) Chaturvedi P, Insana MF, Hall TJ. Testing the limitations of 2-D local companding in strain imaging using phantoms. IEEE Trans Ultrason Ferroelec Freq Control 1998;45:1022–31.
(19) Fatemi M, Greenleaf JF. Ultrasound-stimulated vibroacoustic spectrography. Science 1998;280:82–5.
(20) Sinkus R, Lorenzen J, Schrader D, Lorenzen M, Dargatz M, Holz D. High-resolution tensor MR elastography for breast tumour detection. Phys Med Biol 2000;45(6):1649–64.
(21) Plewes DB, Bishop J, Samani A, Sciarretta J. Visualization and quantification of breast cancer biomechanical properties with magnetic resonance elastography. Phys Med Biol 2000;45(6):1591–1610.
(22) Nightingale K, Soo MS, Nightingale R, Trahey G. Acoustic radiation force impulse imaging: in vivo demonstration of clinical feasibility. Ultrasound Med Biol 2002;28:227–35.
(23) Sandrin L, Tanter M, Catheline S, Fink M. Shear modulus imaging with 2-D transient elastography. IEEE Trans Ultrason Ferroelectr Freq Control 2002;49(4):426–35.
(24) Greenleaf JF, Fatemi M, Insana M. Selected methods for imaging elastic properties of biological tissues. In: Yarmush M. editor. Annual review of biomedical engineering. Vol. 5. Palo Alto (CA); Annu Rev 2003, p. 57–78.
(25) Zhu Y, Hall TJ. A modified block matching method for real-time freehand strain imaging. Ultrason Imag 2002;24:161–76.
(26) Ophir J, Cespedes I, Ponnekanti H, Yazdi Y, Li X. Elastography: a quantitative method for imaging the elasticity of biological tissues. Ultrason Imag 1991;13:111–34.
(27) Plewes DB, Bishop J, Samani A, Sciarretta J. Visualization and quantification of breast cancer biomechanical properties with MR elastography. Phys Med Biol 2000;45:1591–610.
(28) Fatemi M, Greenleaf JF. Ultrasound-stimulated vibroacoustic spectrography. Science 1998;280:82–5.
(29) Yeung F, Levinson SF, Fu D, Parker KJ. Feature-adaptive motion tracking of ultrasound image sequences using a deformable mesh. IEEE Trans Med Imag 1998;17:945–56.
(30) Muthupillai R, Lomas DJ, Rossman PJ, Greenleaf JF, Manduca A, Ehman RL. Magnetic resonance elastography by direct visualization of propagating acoustic strain waves. Science 1995;269(5232):1854–7.
(31) McKnight AL, Kugel JL, Rossman PJ, Manduca A, Hartmann LC, Ehman RL. MR elastography of breast cancer: Preliminary results. Am J Roentgenol 2002;178:1411–7.
(32) Sinkus R, Lorenzen J, Schrader D, Lorenzen M, Dargatz M, Holz D. High resolution tensor MR elastography for breast tumor detection. Phys Med Biol 2000;45(6):1649–64.
(33) Garra BS, Cespedes EI, Ophir J, Spratt SR, Zuurbier RA, Magnant CM, Pennanen MF. Elastography of breast lesions: initial clinical results. Radiology 1997;202:79–86.
(34) Hall TJ, Zhu Y, Spalding CS. In vivo real-time freehand palpation imaging. Ultrasound Med Biol 2003;29(3):427–35.
(35) Hiltawsky KM, Kruger M, Starke C, Heuser L, Ermert H, Jensen A. Freehand ultrasound elastography of breast lesions: Clinical results. Ultrasound Med Biol 2001;27:1461–9.
(36) Lorenzen J, Sinkus R, Lorenzen M, Dargatz M, Leussler C, Roschmann P, Adam G. MR elastography of the breast: Preliminary clinical results. Rofo Fortschr Geb Rontgenstr Neuen Bildgeb Verfahr 2002;174:830–4.
(37) Nightingale K, Soo MS, Nightingale R, Trahey G. Acoustic radiation force impulse imaging: in vivo demonstration of clinical feasibility. Ultrasound Med Biol 2002;28:227–35.
(38) Bercoff J, Chaffai S, Tanter M, Sandrin L, Catheline S, Fink M, Gennisson JL, Meunier M. In vivo breast tumor detection using transient elastography. Ultrasound Med Bio 2003;29(10):1387–96.
(39) Pauly H, Schwan HP. Mechanisms of absorption of ultrasound in liver tissue. J Acoust Soc Am 1971;50:692–9.
(40) Fields S, Dunn F. Correlation of echographic visualizability of tissue with biological composition and physiological state. J Acoust Soc Am 1976;60:1409–12.

(41) Oelze ML, O'Brien WD Jr, Blue JP, Zachary JF. Differentiation and characterization of rat mammary fibroadenomas and 4T1 mouse carcinomas using quantitative ultrasound imaging. IEEE Trans Med Imaging 2004;23:764–71.
(42) Sarvazyan A. Elastic properties of soft tissues. In: Levy, Bass, Stern, editors. Handbook of elastic properties of solids, liquids, and gases. Vol 3. New York (NY): Academic Press; 2001. p. 107–27.
(43) Madsen EL, Sathoff HJ, Zagzebski JA. Ultrasonic shear wave properties of soft tissues and tissuelike materials. J Acoust Soc Am 1983;74:1346–55.
(44) Tschoegl NW. Phenomenological theory of linear viscoelastic behavior. New York (NY): Springer; 1989.
(45) Pellot-Barakat C, Frouin F, Insana MF, Herment A. Ultrasound elastography based on multi-scale estimations of displacement regularized fields. IEEE Trans Med Imag 2004;23:153–63.
(46) Liu J, Abbey CK, Insana MF. Linear approach to axial resolution in elasticity imaging. IEEE Trans Ultrason Ferro Freq Control 2004;51:716–25.
(47) Hall TJ, Zhu Y, Spalding CS. In vivo real-time freehand palpation imaging. Ultrasound Med Biol 2003;29(3):427–35.
(48) Pollack GH. Cells, gells, and the engines of life. Seattle (WA): Ebner & Sons; 2001.
(49) Hall TJ, Bilgen M, Insana MF, Krouskop TA. Phantom materials for elastography. IEEE Trans Ultrason Ferro Freq Control 1997;44:1355–65.
(50) Madsen EL, Frank GR, Krouskop TA, Varghese T, Kallel F, Ophir J. Tissue-mimicking oil-in-gelatin emulsions for use in heterogeneous elastography phantoms. Ultrason Imag 2003;25:17–38.
(51) Ferry JD. Protein gels. Adv Protein Chem 1948;4:1–78.
(52) Ward AG, Courts A. The Science and Technology of Gelatin. New York: Academic Press; 1977.
(53) Granick S. Motions and relaxations of confined liquids. Science 1991;253:1374–9.
(54) Hoffman AS. Conventional and environmentally sensitive hydrogels for medical and industrial use: A review paper. Polym Gels 1991;268:82–7.
(55) Sridhar M, Du H, Pellot-Barakat C, Simon SI, Insana MF. Ultrasonic mechanical relaxation imaging of pH in biopolymers. Proc SPIE 2004;5373:202–11.
(56) Bussink J, Kaanders JHAM, van der Kogel AJ. Tumor hypoxia at the micro-regional level: clinical relevance and predictive value of exogenous and endogenous hypoxic cell markers. Radiother Oncol 2003;67:3–15.
(57) Gilles RJ, Raghunand N, Karczmar GS, Bhujwalla ZM. MRI of the tumor microenvironment. J Magn Res Imag 2002;16:430–50.
(58) Schornack PA, Gillies RJ. Contributions of cell metabolism and H(+) diffusion to the acidic pH of tumors. Neoplasia 2003;5:135–45.
(59) Rofstad EK. Microenvironment-induced cancer metastasis. Int J Radiat Biol 2000;76:589–605.
(60) Yuan J, Narayanan L, Rockwell S, *et al.* Diminished DNA repair and elevated mutagenesis in mammalian cells exposed to hypoxia and low pH. Cancer Res 2000;60:4372–6.
(61) Chapman JD, Englehardt EL, Stobbe CC, *et al.* Measuring hypoxia and predicting tumor radioresistance with nuclear medicine assays. Radiother Oncol 1998;46:229–37.
(62) Haveman J. The influence of pH on the survival after X-radiation of cultured malignant cells. Effects of carbonylbyanide 3-chlorophenylhydrozone. Int J Radiat Biol 1980;37:201–5.
(63) Song CW, Lyons JC, Griffin RJ, *et al.* Increase in thermosensitivity of tumor cells by lowering intracellular pH. Cancer Res 1993;53:1599–601.
(64) Du H, Liu J, Pellot-Barakat C, Insana MF. Optimizing multicompression approaches to strain imaging. IEEE Trans Ultrason Ferro Freq Control (in press).
(65) Sridhar M, Du H, Pellot-Barakat C, Tsou JK, Insana MF. Ultrasonic imaging of biochemical changes in tissues. Proc IEEE Ultrason Symp August 2004 (in press).